Trapping of slow solitons by longitudinal inhomogeneity in high-index photonic crystal fibers

Lægsgaard, Jesper

Published in:
Optical Society of America. Journal B: Optical Physics

Link to article, DOI:
10.1364/JOSAB.28.002617

Publication date:
2011

Document Version
Publisher's PDF, also known as Version of record

Trapping of slow solitons by longitudinal inhomogeneity in high-index photonic crystal fibers

Jesper Lægsgaard

DTU Fotonik, Technical University of Denmark, Building 345v, DK-2800 Kgs. Lyngby, Denmark

Received June 21, 2011; revised August 26, 2011; accepted September 2, 2011;
posted September 9, 2011 (Doc. ID 149558); published October 7, 2011

Soliton propagation in slow-light states of nonuniform high-index photonic crystal fibers (PCFs) is studied numerically by a recently developed time-propagating 1+1*D* equation. It is demonstrated that very slow solitons can be highly stable against even short-period roughness. Soliton trapping by longitudinal inhomogeneities is also found as the soliton velocity decreases due to Raman scattering. Practical limitations and opportunities based on the simulation results are briefly discussed. © 2011 Optical Society of America

OCIS codes: 060.4005, 060.4370, 060.5295, 060.5530, 190.5650, 190.6135.

1. INTRODUCTION

Slow-light states in photonic bandgap structures are of interest for all-optical buffering or processing of optical signals (for a recent review, see [1]). While ideal photonic crystal structures will in principle allow arbitrarily slow propagation, material loss and structural imperfections have been shown to strongly impact the propagation of slow-light states, limiting the slow-down factors obtainable in practice [2,3]. Effects of loss can in principle be mitigated by the implementation of amplification schemes. Structural imperfections, however, will in practice be an unavoidable limitation. Guidance of slow-light has so far been experimentally realized in planar photonic crystals, which are structured on the subwavelength scale and therefore also has disorder effects appearing on that scale. An interesting, although so far hypothetical, alternative is the use of photonic crystal fibers (PCFs) made of high-index materials such as As_2Se_3, which support slow modes in axially uniform waveguides due to the existence of an in-plane photonic bandgap [4]. General experience from fiber drawing and nanowire tapering gives reason to expect that significant inhomogeneity in such fibers would only appear over longer length scales and so it is of interest to study the limitations arising from such fluctuations.

It has recently been suggested that slow-light states in fibers could conveniently be excited by optical solitons, which would asymptotically approach the zero-velocity state due to Raman scattering [5,6]. It is well-known that solitons are relatively stable against long-wavelength perturbations [7,8] and that sufficiently slow solitons may be trapped or reflected by longitudinal inhomogeneities [9]. Recent modeling has studied these processes for slow solitons in quantum two-level media [10] and atomic chains [11]. On the one hand, this indicates that solitons may be stable, even if their propagation is strongly perturbed. On the other hand, it suggests that unintentional imperfections could make it difficult to control the behavior of slow solitons. The purpose of this paper is to model the propagation of slow solitons in a realistic As_2Se_3 fiber design [6], to quantify the effect of weak disorder on soliton stability and propagation.

Because of the high-index contrasts necessary in slow-light fibers of the type investigated here, it is important to develop nonlinear propagation equations whose formulation do not rely on scalar approximations. In a recent paper, a generalized nonlinear Schrödinger equation propagating in the time-domain was developed and used to model soliton propagation in a microstructured As_2Se_3 fiber supporting slow modes around $2\,\mu$m in a small-area solid core [6]. The time-domain propagation formulation is highly advantageous for describing pulses with very slow, and possibly bidirectional, motion in the longitudinal dimension. In this paper, the method is extended to include the effect of longitudinal inhomogeneities and the same fiber design is studied numerically. It is shown that soliton deceleration will eventually lead to trapping of the soliton in some "potential well" of the longitudinal structure. Thus, the inhomogeneity does not in principle limit the slow-down factor, but does severely limit controlled application of slow-light propagation.

2. FORMALISM

The starting point is the Maxwell equations with the displacement term separated into a linear term describing the ideal waveguide and a small perturbation term $\delta\mathbf{P}$:

$$\nabla \times \mathbf{E} = -\mu_0 \frac{\partial \mathbf{H}}{\partial t}, \tag{1}$$

$$\nabla \times \mathbf{H} = \varepsilon_0 \varepsilon(\mathbf{r}_\perp) \frac{\partial \mathbf{E}}{\partial t} + \frac{\partial \delta\mathbf{P}}{\partial t}. \tag{2}$$

In [6], $\delta\mathbf{P}$ was assumed to include only nonlinear terms, but in this paper it will also include a linear term representing deviations from the ideal structure:

$$\delta\mathbf{P} = \varepsilon_0 \delta\varepsilon(\mathbf{r}_\perp, z)\mathbf{E} + \mathbf{P}_{\mathrm{NL}}. \tag{3}$$

Here ε is the relative dielectric constant of the ideal fiber and $\mathbf{P}_{\mathrm{NL}}$ is the nonlinear part of the induced polarization. For high-index contrast structures, $\delta\varepsilon(\mathbf{r}_\perp, z)$ must be considered a tensorial quantity, which is not always related to the structural

perturbations in a simple way [12,13], although for the case of a shifting plane material boundary an analytical expression is readily obtained [14]. In this paper, explicit calculations of the perturbed fields for specific structural perturbations will not be carried out and there is no need to go in further details with this issue. Instead, the fluctuations will be parameterized in a simple way as described below.

The **E** and **H** fields are expanded into modal fields:

$$\mathbf{H}(\mathbf{r},t)=\frac{1}{\sqrt{2\pi}}\sum_m\int \mathrm{d}\beta[(A_m(t,\beta)+\delta_m(t,\beta))\mathbf{h}_m(\mathbf{r}_\perp,\beta)e^{i(\omega_m(\beta)t-\beta z)} + (A_m^*(t,-\beta)+\delta_m^*(t,-\beta))\mathbf{h}_m^*(\mathbf{r}_\perp,-\beta)e^{-i(\omega_m(\beta)t+\beta z)}], \quad (4)$$

$$\mathbf{E}(\mathbf{r},t)=\frac{1}{\sqrt{2\pi}}\sum_m\int \mathrm{d}\beta[A_m(t,\beta)\mathbf{e}_m(\mathbf{r}_\perp,\beta)e^{i(\omega_m(\beta)t-\beta z)} + A_m^*(t,-\beta)\mathbf{e}_m^*(\mathbf{r}_\perp,-\beta)e^{-i(\omega_m(\beta)t+\beta z)}], \quad (5)$$

where the β integration extends over both positive and negative values. The modes $\mathbf{h}_m(\mathbf{r},t;\beta)$, $\mathbf{e}_m(\mathbf{r},t;\beta)$ given by

$$\begin{aligned}\mathbf{h}_m(\mathbf{r},t;\beta)&=\mathbf{h}_m(\mathbf{r}_\perp,\beta)e^{i(\omega_m(\beta)t-\beta z)},\\ \mathbf{e}_m(\mathbf{r},t;\beta)&=\mathbf{e}_m(\mathbf{r}_\perp,\beta)e^{i(\omega_m(\beta)t-\beta z)},\end{aligned} \quad (6)$$

fulfill the linear Maxwell equations for the ideal structure

$$\begin{aligned}\nabla\times\mathbf{e}_m(\mathbf{r},t;\beta)&=-\mu_0\frac{\partial\mathbf{h}_m(\mathbf{r},t;\beta)}{\partial t},\\ \nabla\times\mathbf{h}_m(\mathbf{r},t;\beta)&=\varepsilon_0\varepsilon(\mathbf{r}_\perp)\frac{\partial\mathbf{e}_m(\mathbf{r},t;\beta)}{\partial t},\end{aligned} \quad (7)$$

and are normalized according to

$$\begin{aligned}&\varepsilon_0\int \mathrm{d}\mathbf{r}_\perp\varepsilon(\mathbf{r}_\perp)\mathbf{e}_m^*(\mathbf{r}_\perp,\beta)\cdot\mathbf{e}_n(\mathbf{r}_\perp,\beta)\\ &\quad=\mu_0\int \mathrm{d}\mathbf{r}_\perp\mathbf{h}_m^*(\mathbf{r}_\perp,\beta)\cdot\mathbf{h}_n(\mathbf{r}_\perp,\beta)=\frac{1}{2}\delta_{\mathrm{mn}}.\end{aligned} \quad (8)$$

The time-dependent expansion coefficients $A_m(t,\beta)$ and $\delta_m(t,\beta)$ coefficients are respectively constant and zero for linear propagation in the ideal fiber. When nonlinear effects and/or linear perturbations are added, $A_m(t,\beta)$ aquires a time dependence, and in this case $\delta_m(t,\beta)$ must be nonzero, because both **E**, **H** and **e**, **h** must satisfy Faradays law, Eqs. (1) and (7), respectively. These equations lead to the requirement

$$\frac{\partial A_m(t,\beta)}{\partial t}=-i\omega_m(\beta)\delta_m(t,\beta)-\frac{\partial\delta_m(t,\beta)}{\partial t}, \quad (9)$$

which specifies the connection between $A_m(t,\beta)$ and $\delta_m(t,\beta)$. It is important to note that Eq. (9) is a consequence of the choice of basis states in Eqs. (4) and (5), and might appear different in formulations based on other expansions.

The central assumption underlying the following derivations is that $|\partial A_m(t,\beta)/\partial t|\ll\omega(\beta)|A_m(t,\beta)|$, i.e. the field expansion coefficients vary slowly compared to the optical frequencies. It is then natural to neglect the time derivative of $\delta_m(t,\beta)$ in Eq. (9) compared to the term $-i\omega_m(\beta)\delta_m(t,\beta)$. This is because a rapidly oscillating term in $\delta_m(t,\beta)$ would tend to average out over the slower time scale of $A_m(t,\beta)$ variations, whereas a rapid growth or decay in the amplitude of $\delta_m(t,\beta)$ would be difficult to reconcile with Eq. (9) under the assumption of a small $\partial A_m(t,\beta)/\partial t$. Neglecting the time derivative of $\delta_m(t,\beta)$, one obtains

$$\frac{\partial A_m(t,\beta)}{\partial t}\approx-i\omega_m(\beta)\delta_m(t,\beta)\Rightarrow\delta_m(t,\beta)\approx\frac{i}{\omega_m(\beta)}\frac{\partial A_m(t,\beta)}{\partial t}. \quad (10)$$

With this expression, the time derivative of $\delta_m(t,\beta)$ becomes

$$\frac{\partial\delta_m(t,\beta)}{\partial t}=\frac{i}{\omega(\beta)}\frac{\partial^2A_m(t,\beta)}{\partial t^2}. \quad (11)$$

Thus, the neglect of $\partial\delta_m(t,\beta)/\partial t$ can also be thought of as a neglect of the second time derivative of $A_m(t,\beta)$, an assumption which is commonly used in scalar z- or t-propagating derivations [15].

Since the $A_m(t,\beta)$ are constant in the linear case, they can be expected to be slowly varying for sufficiently weak linear and nonlinear perturbations. On the other hand, the assumption does not limit the pulse duration, which can in principle be very short even with slowly varying $A_m(t,\beta)$ coefficients, if they extend over a broad bandwidth. Using Eq. (10) along with the Maxwell equations and eigenmode expansions discussed above, one may derive the propagation equation [6]

$$\frac{\partial A_m(t,\beta)}{\partial t}=-\frac{1}{\sqrt{2\pi}}\int \mathrm{d}\mathbf{r}\mathbf{e}_m^*(\mathbf{r},t;\beta)\cdot\frac{\partial\delta\mathbf{P}^+}{\partial t}. \quad (12)$$

Here $\frac{\partial\delta\mathbf{P}^+}{\partial t}$ denotes that part of $\delta\mathbf{P}$ which oscillates at positive frequencies. This is a very general equation, from which one can derive both nonlinear Schrödinger-type equations and linear or nonlinear coupled-mode equations, depending on the number of eigenstates in the expansion, and the nature of the $\delta\mathbf{P}$ term.

Consider the linear part of $\delta\mathbf{P}^+$, as given by Eq. (3). The overlap with $\mathbf{e}^*$ on the RHS of Eq. (12) can be evaluated to

$$\begin{aligned}&\int \mathrm{d}\mathbf{r}\mathbf{e}_m^*(\mathbf{r},t;\beta)\cdot\varepsilon_0\delta\varepsilon(\mathbf{r}_\perp,z)\frac{\partial\mathbf{E}(\mathbf{r},t)}{\partial t}\approx\frac{1}{\sqrt{2\pi}}\int \mathrm{d}z e^{i(\beta z-\omega_m(\beta)t)}\\ &\times\frac{1}{\sqrt{2\pi}}\int \mathrm{d}\beta_1 i\omega_n(\beta_1)e^{i(\omega_n(\beta_1)t-\beta_1 z)}A(t,\beta_1)\\ &\times\int \mathrm{d}\mathbf{r}_\perp\varepsilon_0\delta\varepsilon(\mathbf{r}_\perp,z)\mathbf{e}_m^*(\mathbf{r}_\perp,-\beta)\cdot\mathbf{e}_n(\mathbf{r}_\perp,\beta_1)\approx e^{-i\omega_m(\beta)t}\\ &\times\int \mathrm{d}z e^{i\beta z}B_n(t,z)\Delta_{\mathrm{mn}}(z).\end{aligned} \quad (13)$$

Here $\Delta_{\mathrm{mn}}(z)$ describes the overlap integral of the modal field and the perturbation,

$$\Delta_{\mathrm{mn}}(z)=\int \mathrm{d}\mathbf{r}_\perp\varepsilon_0\delta\varepsilon(\mathbf{r}_\perp,z)\mathbf{e}_m^*(\mathbf{r}_\perp,\beta=0)\cdot\mathbf{e}_n(\mathbf{r}_\perp,\beta=0). \quad (14)$$

The function $B_m(t,z)$ is given by

$$\begin{aligned}B_m(t,z)&=\frac{1}{\sqrt{2\pi}}\int \mathrm{d}\beta e^{-i\beta z}i\omega_m(\beta)\tilde{A}_m(t,\beta)\\ &=\frac{1}{\sqrt{2\pi}}\int \mathrm{d}\beta e^{-i\beta z}i\omega_m(\beta)A_m(t,\beta)e^{i\omega_m(\beta)t}\end{aligned} \quad (15)$$

and is approximately equal to $i\omega_m(0)\tilde{A}_m(t,z)$ if the variation of ω_m with β is ignored. In the first equality in Eq. (13), the time derivative of $A_n(t,\beta)$ was neglected in comparison with $i\omega_n(\beta)A_n(t,\beta)$. This is consistent with the assumption that $\delta\mathbf{P}$ is weak, since A_n would be constant in the absence of $\delta\mathbf{P}$. In the last step, the mode profile dispersion was neglected. This approximation can straightforwardly be improved, *e.g.* by expanding the modal fields in powers of β. As an example, a first-order expansion of the form

$$\mathbf{e}_n(\mathbf{r}_\perp,\beta) \approx \mathbf{e}_n(\mathbf{r}_\perp,\beta=0) + \beta\mathbf{e}_n^{(1)}(\mathbf{r}_\perp) \tag{16}$$

would yield the linear $\delta\mathbf{P}^+$ contribution

$$\begin{aligned}&\int \mathrm{d}\mathbf{r}\mathbf{e}_m^*(\mathbf{r},t;\beta)\cdot\varepsilon_0\delta\varepsilon(\mathbf{r}_\perp,z)\frac{\partial\mathbf{E}(\mathbf{r},t)}{\partial t}\\ &\approx e^{-i\omega_m(\beta)t}\int \mathrm{d}z e^{i\beta z}\Big[B_n(t,z)(\Delta_{\mathrm{mn}}(z)-\beta\Delta_{\mathrm{nm}}'^*(z))\\ &\quad-\Delta_{\mathrm{mn}}'(z)\frac{\partial B_n(t,z)}{\partial z}\Big],\end{aligned} \tag{17}$$

with an additional complex overlap term $\Delta_{\mathrm{mn}}'(z)$ given by

$$\Delta_{\mathrm{mn}}'(z) = \int \mathrm{d}\mathbf{r}_\perp\varepsilon_0\delta\varepsilon(\mathbf{r}_\perp,z)\mathbf{e}_m^*(\mathbf{r}_\perp,\beta=0)\cdot\mathbf{e}_n^{(1)}(\mathbf{r}_\perp). \tag{18}$$

Since in this paper, the inhomogeneity will be parameterized in a phenomenological way, only the Δ_{mn} term will be retained in the following, to simplify the parametrization. A few test calculations incorporating a correction of the form (17) did not indicate that this correction added new qualitative trends, although this subject has not been exhaustively investigated.

In the following, it will further be assumed that only one fiber mode needs to be included in the calculations and the mn indices on envelope functions, frequencies, etc. will therefore be suppressed. With this approximation, the modeling does not describe scattering of the slow solitons into other guided modes, or cladding modes, of the fiber. It does, however, describe scattering of soliton power into dispersive waves, and also backscattering into the slow mode itself. In planar slow-light devices, the latter effect has been found to constitute the dominant loss mechanism at low group velocities [2].

Inserting the nonlinear polarization term derived in [6], Eq. (12) becomes

$$\begin{aligned}\frac{\partial A(t,\beta)}{\partial t} = -e^{-i\omega(\beta)t}\frac{1}{\sqrt{2\pi}}\int \mathrm{d}z e^{i\beta z}\Big[&\frac{N_2}{A_{\mathrm{eff}}}\{(1\\ &-f_R)(2|\tilde{A}(t,z)|^2B(t,z)+\tilde{A}^2(t,z)B^*(t,z))\\ &+f_R(\tilde{A}(t,z)G(t,z)+B(t,z)F(t,z))\}\\ &+B(t,z)\Delta(z)\Big].\end{aligned} \tag{19}$$

The functions F and G describe the Raman interaction which appears in a different form than for z-stepping formalisms because the Raman interaction is nonlocal in time, but not in space. They are given by

$$\begin{aligned}F(t,z) &= \int_{-\infty}^{t}\mathrm{d}t_1 R(t-t_1)|\tilde{A}(t_1,z)|^2,\\ G(t,z) &= \int_{-\infty}^{t}\mathrm{d}t_1 R'(t-t_1)|\tilde{A}(t_1,z)|^2.\end{aligned} \tag{20}$$

The nonlinear parameters N_2 and f_R are given in terms of the $\chi^{(3)}$ constants by

$$N_2 = \frac{3\chi_s^{(3)}}{4\varepsilon_0\varepsilon_m^2}; \qquad \chi_s^{(3)} = \chi_{Kxxxx}^{(3)} + \frac{2}{3}\chi_{Rxxxx}^{(3)}; \qquad f_R = \frac{2\chi_{Rxxxx}^{(3)}}{3\chi_s^{(3)}}. \tag{21}$$

The Raman response function, $R(t)$ will in this paper be parameterized as the interaction of the optical field with a single damped oscillator [15],

$$R(t) = \frac{\tau_1^2+\tau_2^2}{\tau_1\tau_2^2}\sin\left(\frac{t}{\tau_1}\right)e^{-\frac{t}{\tau_2}}. \tag{22}$$

As discussed in [6], this allows for a convenient determination of the F and G functions during the numerical calculations.

Transforming the propagation equation into the z-domain, recasting it as an equation for $\tilde{A}$, neglecting the nonlinear terms, and assuming $B(t,z)\approx i\omega(0)\tilde{A}(t,z)$ yields the propagation equation

$$-i\frac{\partial\tilde{A}(t,z)}{\partial t} = \omega_0[1-\Delta(z)]\tilde{A}(t,z) - \frac{\omega_2}{2}\frac{\partial^2\tilde{A}(t,z)}{\partial z^2}, \tag{23}$$

which is seen to be identical to the quantum mechanical Schrödinger equation, with $-\omega_0\Delta(z)$ acting as a potential term. Thus, a moving soliton (or other wavepacket) will be slowed down when $\Delta(z)$ decreases and accelerated when $\Delta(z)$ increases. In optics language, the local eigenmodes at some value of z where the fiber cross section is perturbed by $\delta\varepsilon(\mathbf{r}_\perp,z)$ will have the $\beta=0$ eigenfrequency shifted by a $\delta\omega$ given by

$$\frac{\delta\omega}{\omega} = -\int \mathrm{d}\mathbf{r}_\perp\varepsilon_0\delta\varepsilon(\mathbf{r}_\perp,z)|\mathbf{e}(\mathbf{r}_\perp,\beta=0)|^2 = -\Delta(z) \tag{24}$$

in first-order perturbation theory [12]. Thus, in the simplest approximation, the perturbation can be imagined to shift the $\omega(\beta)$ curve up or down, depending on the sign of $\Delta(z)$. However, in the linear regime the frequency of the pulse cannot change, and so its propagation constant, and hence its velocity, must change instead (which is possible, because the translational symmetry along z is broken by the perturbation). If the frequency curve is shifted upwards (negative $\Delta(z)$), the propagation constant must decrease and vice versa. If the frequency curve is shifted high enough that $\omega(0)$ becomes larger than the pulse frequency, the pulse cannot propagate further and reflection must be expected. In the quantum mechanics analogue, this would correspond to hitting an insurmountable potential barrier. From this consideration a simple criterion for an impenetrable $\Delta(z)$ value may be derived:

$$\frac{\delta\omega}{\omega} = -\Delta(z) > \frac{\omega(\beta)-\omega_0}{\omega} = \frac{\frac{\omega_2}{2}\beta^2}{\omega_0+\frac{\omega_2}{2}\beta^2} \approx \frac{\omega_2}{2\omega_0}\beta^2. \tag{25}$$

3. NUMERICAL RESULTS AND DISCUSSION

In the numerical simulations, the same fiber parameters as in [6] were used. Thus $\omega(\beta)$ is given by

$$\omega(\beta) = \omega_0 + \omega_2\beta^2, \qquad \omega_0 = \frac{2\pi c}{\lambda_0}, \tag{26}$$

with $\lambda_0 = 1.989\,\mu$m and $\omega_2 = 26.23\,\mu\text{m}^2/\text{ps}$. The effective area was set to $= 1.7\,\mu\text{m}^2$ and the Raman response function parameters were taken as $\tau_1 = 23$ fs, $\tau_2 = 230$ fs, $f_R = 0.2$. The nonlinear coefficient of As_2Se_3 at a wavelength of $\sim 2\,\mu$m was assumed to be $6\times10^{-6}\,\mu\text{m}^2/\text{W}$, from which $\chi^{(3)}$ and thereby N_2 was calculated. The simulations were performed on a z-grid with a discretization step of $0.5\,\mu$m.

With these parameters, a pulse with $\beta \approx \mu\text{m}^{-1}$ will have a group velocity $v_g \approx 0.087c$. If the pulse moves at this velocity for $\Delta(z) = 0$, it will be unable to penetrate a $\Delta(z) < -0.0138$. This critical barrier height will be proportional to β^2 and therefore v_g^2. In the following $\Delta(z)$ magnitudes significantly below 10^{-2} will be investigated.

A. Periodic Perturbation

The response of a soliton to a weak periodic perturbation is well-studied and is experimentally clearly seen as the formation of Kelly sidebands in solitonic fiber lasers [7,8]. Below, a brief derivation of the key results is presented using the notation of the present paper. A nonlinear Schrödinger equation equation without Raman and self-steepening terms will be used. Consider a cosine perturbation with magnitude $\delta\omega$ and wave vector $K = 2\pi/L_p$ and assume that a soliton couples to a weak dispersive wave with propagation constant β_d:

$$A(t,\beta) = A_s(t,\beta) + \delta A(t,\beta), \tag{27}$$

$A_s(t,\beta)$ is the soliton waveform in reciprocal space,

$$A_s(t,\beta) = \frac{1}{\sqrt{2\pi}}\int \mathrm{d}z \exp^{-i\beta z} A_s(t,z), \tag{28}$$

with the real-space waveform being

$$A_s(t,z) = \sqrt{\xi_0}\,\mathrm{sech}\left(\frac{z-v_g t}{z_0}\right) e^{it(\omega(\beta_s)-1/T_{\mathrm{NL}})} e^{-i\beta_s z}. \tag{29}$$

The nonlinear coefficient Γ and the soliton parameters z_0 and T_{NL} are given by

$$z_0^2 = \frac{\omega_2}{\Gamma\xi_0}; \qquad \Gamma = \frac{\omega_0 N_2}{A_{\mathrm{eff}}}; \qquad T_{\mathrm{NL}} = \frac{1}{\Gamma\xi_0}. \tag{30}$$

The dispersive wave $\delta A(t,\beta)$ is assumed to be strongly peaked around β_d. The time evolution of δA is found to be

$$\begin{aligned}\frac{\partial\delta A(t,\beta_d)}{\partial t} = \frac{i}{\sqrt{2}}\int \mathrm{d}z \{ & e^{it(\omega(\beta_s)-1/2T_{\mathrm{NL}}-\omega(\beta_d))} e^{iz(\beta_d-\beta_s)} \frac{\delta\omega}{2}(e^{iKz} \\ & + e^{-iKz})\sqrt{\xi_0}\,\mathrm{sech}\left(\frac{z-v_g t}{z_0}\right) \\ & + \Gamma e^{i(\beta_d z-\omega(\beta_d)t)}[2|\tilde{A}_s(t,z)|^2\delta\tilde{A}(t,z) \\ & + \tilde{A}_s^2\delta\tilde{A}^*(t,z)]\}. \end{aligned} \tag{31}$$

If the dispersive wave is extended compared to the soliton, its nonlinear interaction with the soliton will be negligible. The first term in Eq. (31) can be rewritten as

$$\begin{aligned} & \frac{i}{\sqrt{2}} e^{it(\omega(\beta_s)-1/2T_{\mathrm{NL}}-\omega(\beta_d))} \int \mathrm{d}z e^{iz(\beta_d-\beta_s)} \frac{\delta\omega}{2}(e^{iKz} \\ & \quad + e^{-iKz})\sqrt{\xi_0}\,\mathrm{sech}\left(\frac{z-v_g t}{z_0}\right) \\ & = \frac{i}{\sqrt{2}} e^{it(\omega(\beta_s)-1/2T_{\mathrm{NL}}-\omega(\beta_d)+v_g(\beta_d-\beta_s))} \int \mathrm{d}u e^{iu(\beta_d-\beta_s)} \frac{\delta\omega}{2}(e^{iKv_g t}e^{iKu} \\ & \quad + e^{-iKv_g t}e^{-iKu})\sqrt{\xi_0}\,\mathrm{sech}\left(\frac{u}{z_0}\right) \\ & = \frac{i}{\sqrt{2}} e^{it(\omega(\beta_s)-1/2T_{\mathrm{NL}}-\omega(\beta_d)+v_g(\beta_d-\beta_s))}\sqrt{\xi_0} \\ & \quad \times \left[e^{iKv_g t}\,\mathrm{sech}\left(\frac{\pi}{2}(\beta_d-\beta_s+K)z_0\right)\right. \\ & \quad \left. + e^{-iKv_g t}\,\mathrm{sech}\left(\frac{\pi}{2}(\beta_d-\beta_s-K)z_0\right)\right]. \end{aligned} \tag{32}$$

Resonant transfer of energy from the soliton into the dispersive wave will occur when

$$\omega(\beta_s) - \frac{1}{2}T_{\mathrm{NL}} - \omega(\beta_d) + v_g(\beta_d-\beta_s) \pm Kv_g = 0. \tag{33}$$

Using the relations $\omega(\beta) = \omega_0 + \frac{1}{2}\omega_2\beta^2$ and $v_g = \omega_2\beta_s$ this becomes

$$\begin{aligned} & \frac{1}{2}\omega_2(\beta_s^2-\beta_d^2) + \omega_2\beta_s(\beta_d-\beta_s) \pm Kv_g - \frac{1}{2}T_{\mathrm{NL}} \\ & \quad = -\frac{1}{2}\omega_2(\beta_s-\beta_d)^2 \pm Kv_g - \frac{1}{2}T_{\mathrm{NL}} = 0. \end{aligned} \tag{34}$$

Finally, introducing the soliton spatial width z_0 through Eq. (30) one arrives at

$$(\beta_d-\beta_s)^2 = \pm 2K\beta_s - z_0^{-2} = z_0^{-2}\left(\frac{4\pi v_g T_{\mathrm{NL}}}{L_p} - 1\right), \tag{35}$$

where the last step follows from the fact that the LHS is positive definite. It is evident that if $L_p > 4\pi v_g T_{\mathrm{NL}}$, the resonance condition is not satisfied for real β_d.

A numerical test of the analytical predictions is illustrated in Fig. 1. A perturbation of the form

$$\Delta(z) = \Delta_0\cos(Kz), \qquad K = \frac{2\pi}{L_p} \tag{36}$$

was introduced with $\Delta_0 = 10^{-4}$ and 10^{-3},respectively. An ideal soliton with a peak energy density of $15\,\text{pJ}/\mu$m was launched at $z = 0$ and propagated for 500 ps. Raman effects were

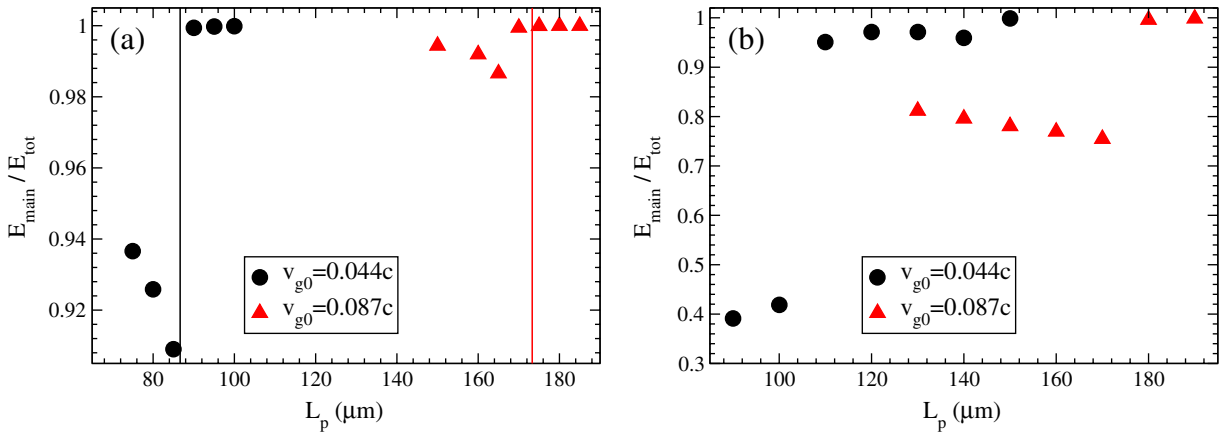

Fig. 1. (Color online) Fraction of pulse energy in main peak after 500 ps of propagation for various periods of a cosine $\Delta(z)$. (a) Results for a $\Delta(z)$ magnitude of 10^{-4}, (b) results for a magnitude of 10^{-3}.

neglected for the sake of comparison with the analytical prediction. At the end of the propagation, it was determined how much pulse power remained in the main peak of the pulse. Two values of β_s were investigated, $\beta_s = 1\,\mu\text{m}^{-1}$ and $\beta_s = 0.5\,\mu\text{m}^{-1}$, corresponding to group velocities of $0.087c$ and $0.044c$, respectively. In Fig. 1, which shows the results for $\Delta_0 = 10^{-4}$, vertical lines indicate the analytical predictions for the L_p values above which the soliton should become robust against the perturbation and it is seen that they match very well with the numerical results. For $\Delta_0 = 10^{-3}$, the threshold L_p value is seen to shift significantly for the soliton with $\beta_s = 0.5\,\mu\text{m}^{-1}$, showing that the soliton shape varies significantly during propagation, so that the perturbative analysis becomes invalid. In Fig. 2, the fluctuations in peak intensity are depicted for $\Delta_0 = 10^{-3}$ and two values of L_p above the threshold where the soliton is stable. The fluctuations can be understood by noting that the soliton accelerates for increasing values of $\Delta(z)$, and vice versa, as discussed in the previous section. An accelerating soliton is stretched in space since its leading edge aquires a higher velocity than its trailing edge. Conversely, a decelerating soliton is compressed spatially. In Fig. 2, the variation in peak intensity is seen to become stronger when the period of $\Delta(z)$ is shortened because the acceleration and deceleration caused by the fluctuations thereby become larger.

In Fig. 1, it may be noticed that the soliton scattering tends to be stronger as L_p moves closer to the threshold value where scattering is cut off. This can be understood from Eq. (32), which shows that for small $\beta_d - \beta_s$ the scattering intensity will be proportional to $\text{sech}(Kz_0)$. From Eq. (35) $\beta_d - \beta_s$ will be small in the vicinity of the threshold L_p value. If L_p is made very small, $\beta_d - \beta_s \approx \sqrt{2K\beta_s}$, so $\text{sech}((\beta_d - \beta_s \pm K)z_0) \approx \text{sech}(Kz_0)$ is a reasonable first approximation also when $K \gg \beta_s$. In Fig. 3, an example with $L_p = 2.5\,\mu\text{m}$ ($K \approx 2.5\,\mu\text{m}^{-1}$), $\Delta_0 = 4 \cdot 10^{-3}$, $\beta_s = 0.5\,\mu\text{m}^{-1}$ is shown (other parameters as in Fig. 1). Clearly, this example is not in the perturbative regime: the peak energy density of the soliton is seen to have significant fluctuations and the pulse after 500 ps deviates strongly from the ideal soliton form. Nevertheless, a pulse with a FWHM close to the starting value of ~6.5 μm (corresponding to $z_0 \approx 3.7$) is retained, with less than 10% of the total energy lost to dispersive waves.

It follows from the above discussion that $L_p \lesssim z_0$ may be taken as a rough criterion for low scattering magnitude, altough there is not a threshold effect as in the opposite limit of large L_p. If z_0 is larger than the L_p threshold value $4\pi v_g T_{\text{NL}}$ that follows from Eq. (35), the soliton should then be immune to scattering from perturbations of *all* wavelengths. This requirement can be rewritten as

$$z_0 \gtrsim 4\pi v_g T_{\text{NL}} \Rightarrow z_0 \gtrsim \frac{4\pi v_g z_0^2}{\omega_2} \Rightarrow 4\pi\beta_s z_0 \lesssim 1. \qquad (37)$$

Since the soliton amplitude in reciprocal space is proportional to $\text{sech}(\pi(\beta - \beta_s)z_0/2)$, this requirement basically states that the β-space width of the soliton is larger than the magnitude of β_s, *i.e.* the soliton should have appreciable components of both forward- and backward-propagating waves. This is exactly the regime where unidirectional z-propagating schemes become inadequate.

B. Random Structural Fluctuations

In a real fiber, the structural fluctuations will be random and will in principle have contributions from all Fourier components. It is therefore not obvious that the existence of a threshold periodicity for soliton scattering has any practical relevance. In this subsection, propagation along a fiber perturbed by a random $\Delta(z)$ is therefore investigated. Since our knowledge of the actual fluctuation spectrum in a fiber

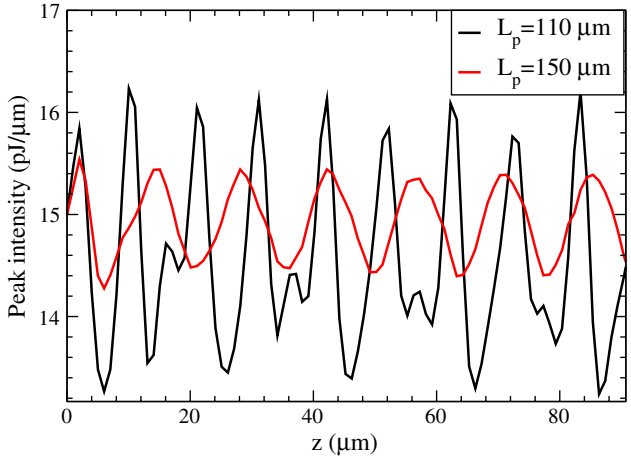

Fig. 2. (Color online) Peak intensity of soliton as a function of propagation distance for a cosine $\Delta(z)$ of magnitude 10^{-3}. The initial soliton velocity is $0.044\,c$.

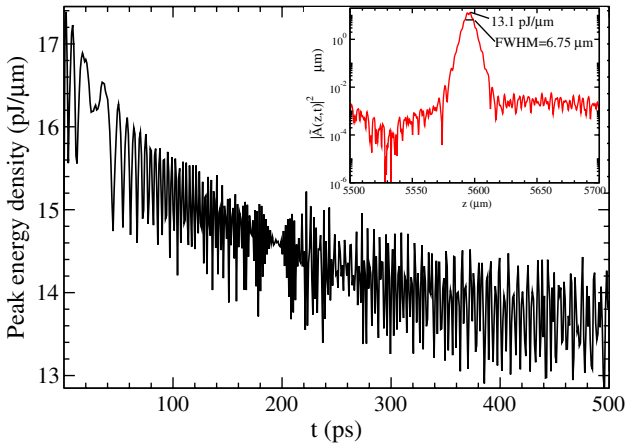

Fig. 3. (Color online) Peak intensity of soliton as a function of propagation distance for a cosine $\Delta(z)$ of magnitude $4\cdot10^{-3}$ and $L_p = 2.5\,\mu$m. Inset shows the pulse shape after 500 ps propagation. The initial soliton velocity is $0.044c$ and initial energy density is $15\,\mathrm{pJ}/\mu\mathrm{m}$.

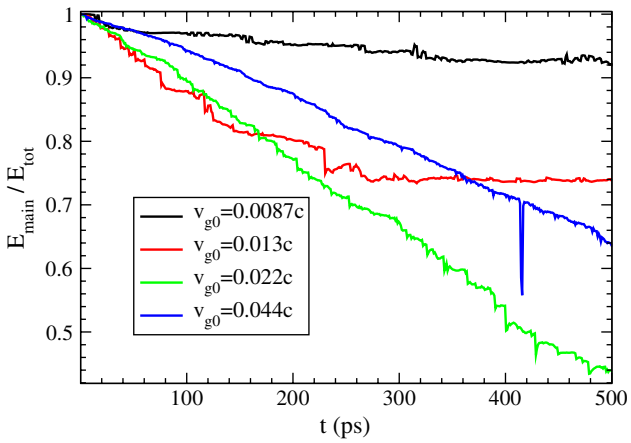

Fig. 5. (Color online) Ratio of energy in soliton main peak E_{main} to total pulse energy E_{tot} versus propagation time for solitons with different initial velocities propagating in a Gaussian disorder field with $L_c = 0.5\,\mu$m and RMS width 10^{-4}. Other parameters as in Fig. 4.

is limited, especially for a fiber type which has not yet been fabricated, a Gaussian fluctuation spectrum is adopted here, with

$$\Delta(z) = \Delta_0 \sum_m \Phi_m \exp\left(-\frac{1}{2}k_m^2\left(\frac{L_c}{2}\right)^2\right)\exp(ik_m z),$$
$$k_m = \frac{2\pi m}{L}, \tag{38}$$

where L is the length of the z-domain used in the calculation. Here the Φ_m are random phase factors, whereas the amplitude of the fluctuations can be adjusted by the overall Δ_0 factor. L_c can be regarded as a correlation length for the structural fluctuations [16]. In the numerical calculations, the $\Delta(z)$ function calculated from Eq. (38) is shifted to be zero at $z = 0$, where the soliton is launched and then rescaled so that the root-mean-square (RMS) deviation from its mean is equal to a desired value. This implies that the mean value of $\Delta(z)$ may be different from zero. Two realization examples are shown in Fig. 4(a) for an RMS width of 10^{-3}. In Fig. 4(b), the energy fraction remaining in the main soliton peak after 500 ps of propagation is plotted versus L_c for the same RMS value. The soliton peak intensity was $15\,\mathrm{pJ}/\mu\mathrm{m}$ as in the previous subsection, however, in this case Raman scattering was included in the calculations. For each L_c value, four different realizations of the random structure were investigated. The randomness smoothens out the transition between scattering and nonscattering regimes a bit, but an approximate threshold is still noticeable.

In the previous subsection, it was suggested that very slow solitons could be relatively immune to scattering from all Fourier components of the disorder. In Fig. 5, this hypothesis is tested by propagating solitons with different initial velocities in a $\Delta(z)$ structure having Gaussian randomness with $L_c = 0.5\,\mu$m, which is identical to the real-space Fourier grid spacing and a RMS width of 10^{-4}. The figure reports the fraction of energy remaining in the soliton as a function of propagation time. It can be seen that the scattering rate initially increases as the velocity is reduced, but that still further reduction reverses the trend, and at velocities below $0.01c$ the soliton is fairly well preserved over several hundred picoseconds, corresponding to about 1 mm of propagation. Interestingly, the slowest soliton has $z_0 \approx 3.7$ and $\beta_s = 0.1\,\mu\mathrm{m}^{-1}$, so that $4\pi\beta_s z_0 \approx 4.6$, i.e., the crude stability criterion derived in the previous subsection is quite far from being fulfilled. If the white-noise magnitude is increased to an RMS width of 10^{-3}, stronger scattering and a much more fluctuating pulse profile

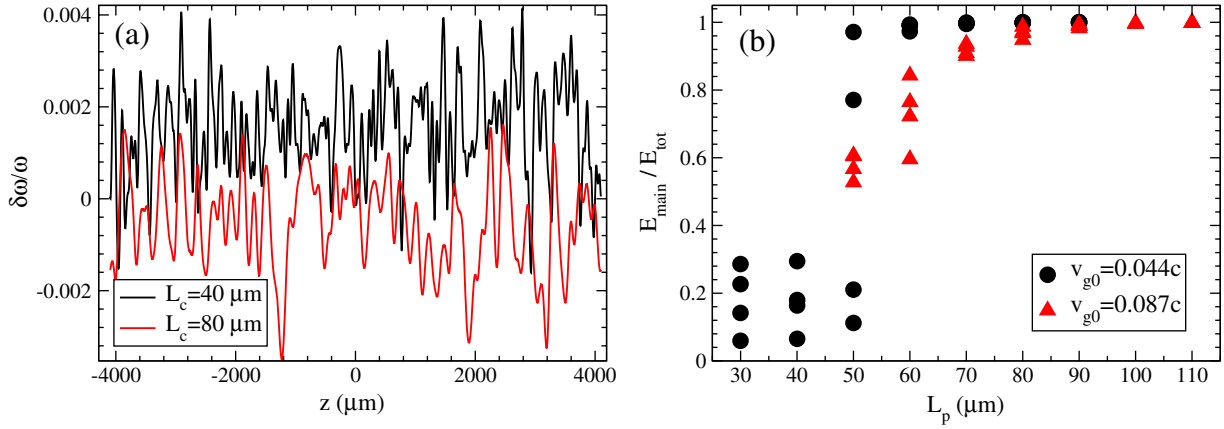

Fig. 4. (Color online) (a) Two examples of random $\Delta(z)$ distributions with Gaussian disorder. The RMS value of $\Delta(z)$ is 10^{-3}. (b) Fraction of pulse energy in main peak after 500 ps of propagation for various values of L_c. For each L_c value, four different realizations of the random structure were investigated.

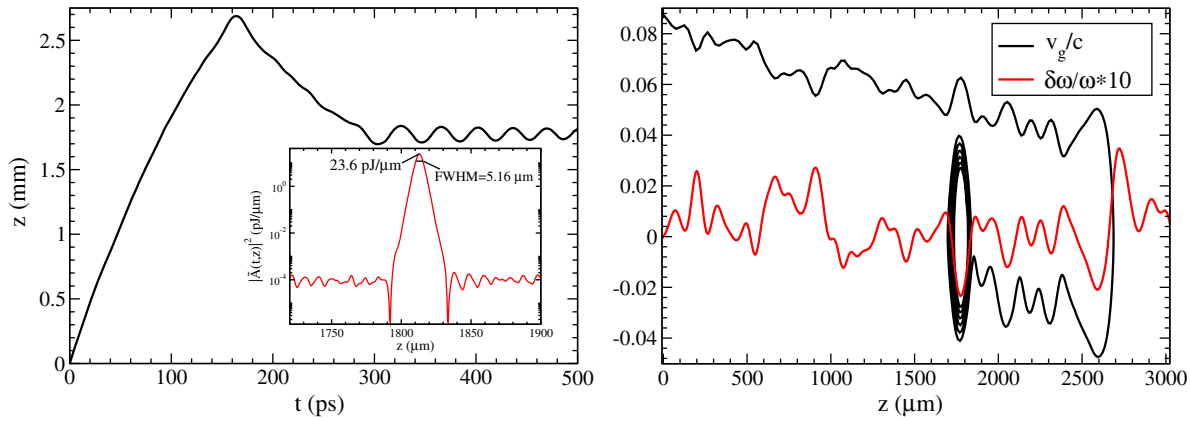

Fig. 6. (Color online) (a) Soliton position as a function of time, in a Gaussian $\Delta(z)$ with RMS $= 10^{-3}$. Inset shows the spatial intensity of the final soliton on a logarithmic scale. (b) Soliton velocity plotted together with $\Delta(z)$, scaled to facilitate comparison.

is seen, but the basic trend of reduced scattering for very slow pulses holds up and the soliton with initial $v_g = 0.013c$ retains ~70% of the total energy in the main peak after 500 ps. In this regime of stronger scattering the slowest solitons are also found to localize, propagating no further than ~10 μm from their starting point.

C. Raman-Induced Soliton Localization

The inclusion of Raman scattering leads to a downshifting of the soliton frequency and thereby an approach towards the $\beta = 0$ state [5,6]. This slowing down in turn implies that it gets increasingly difficult for the soliton to overcome the barriers present in the 'potential' landscape presented by the random $\Delta(z)$ function. This can eventually lead to both reflection and localization of the soliton in some 'potential well' of the fiber. An example is illustrated in Fig. 6. The initial soliton peak intensity has been increased to 25 pJ/μm, to enhance the Raman scattering. The initial β_s is 1 μm^{-1}, $L_c = 60\,\mu$m and the RMS width of the fluctuations is again 10^{-3}. In Fig. 6(a), the z-position of the pulse is plotted as a function of time and in Fig. 6(b), the pulse velocity is plotted as a function of z, together with $\delta\omega/\omega = -\Delta(z)$, scaled to facilitate comparison. The pulse velocity is seen to fluctuate corresponding to the fluctuations in $\delta\omega/\omega$, while decreasing due to Raman scattering. After about 2.7 mm of propagation, the soliton hits a barrier that it cannot pass, due to the reduced velocity. The soliton is then reflected and travels backward while further reducing its velocity. Eventually, the soliton is trapped in a local minimum of $\delta\omega/\omega$, where it goes back and forth with decreasing velocity. The inset of Fig. 6 shows the spatial profile of the soliton after 500 ps propagation and it is seen to be in a more or less intact shape, with very little energy lost to dispersive waves, and a peak intensity close to the starting value.

D. Discussion

The results presented shows two major trends regarding the stability of slow solitons: On the one hand, the scattering of solitons by roughness of a certain magnitude becomes stronger when the soliton slows down, but at the same time the range of fluctuations periods affecting the soliton decreases. Depending on the details of the roughness spectrum, it seems conceivable that very slow localized solitons might exist for a substantial time in a slow-light photonic bandgap fiber. At the same time, Raman scattering constitutes a convenient mechanism for achieving the localization behavior. On the other hand, even if slow-moving solitons can be kept stable, the results found here seem to complicate *controlled* applications of solitons moving at speeds of $0.1c$ or smaller. Even small unintended structural fluctuations will affect the soliton propagation in a way that is not controlled by the fiber designer. To put the numerical results into perspective, it is useful to consider a perturbation which is just an overall scaling of the fiber structure. In this case, the scale invariance of Maxwells equations ensures that the relative change in frequency (*i.e.* $-\Delta(z)$) will be equal to the relative change in overall scale. In [6], it was found that a fiber structure with a 1 μm periodicity of the cladding leads to a useful bandgap around 2 μm. Thus, a $\Delta(z)$ magnitude of 10^{-3} would correspond to a 1 nm fluctuation. While it has been found that standard fibers may have outer-diameter variations of this magnitude over centimeter length scales [17], it is not clear whether a similar level of uniformity can be achieved in the complex microstructures studied here.

However, the findings also point to some technological possibilities using this type of fiber. The high sensitivity of pulse propagation to even small modifications of the fiber structure is unparalleled in standard fiber technology. Working with light states sufficiently fast to avoid trapping and backscattering from uncontrolled imperfections, this degree of propagation control could be useful for *e.g.* reflection filters or tunable delay lines, which could be controlled nonlinearly by the Raman effect.

4. CONCLUSION

In conclusion, a recently derived time-propagating generalized nonlinear Schrödinger equation has been generalized to the case of a longitudinally structured waveguide and applied to the case of slow solitons in a high-index PCF with structural fluctuations. It is shown that the fluctuations scatter solitons into forward- and backward-propagating dispersive waves, unless the soliton velocity is below a threshold related to the periodicity of the fluctuation. Above this threshold, slow solitons are scattered more strongly than fast solitons, except for very slow solitons where the trend is reversed. Even structural fluctuations on the per mill level are found to significantly influence soliton propagation. Soliton deceleration due to the Raman effect is shown to enable

soliton localization in 'potential wells' of the fluctuating longitudinal fiber structure. The results indicate that solitons localized by a combination of disorder and nonlinear effects may well be observable, but also that utilization of the slow pulses in a controlled way may be compromised by finite fabrication tolerances.

REFERENCES

1. T. Baba, "Slow light in photonic crystals," Nat. Photon. **2**, 465–473 (2008).
2. L. O'Faolain, S. A. Schulz, D. M. Beggs, T. P. White, M. Spasenovic, L. Kuipers, F. Morichetti, A. Melloni, S. Mazoyer, J. P. Hugonin, P. Lalanne, and T. F. Krauss, "Loss engineered slow light waveguides," Opt. Express **18**, 27627–27638 (2010).
3. J. G. Pedersen, S. Xiao, and N. A. Mortensen, "Limits of slow light in photonic crystals," Phys. Rev. B **78**, 153101 (2008).
4. A. F. Oskooi, J. D. Joannopoulos, and S. G. Johnson, "Zero—group-velocity modes in chalcogenide holey photonic-crystal fibers," Opt. Express **17**, 10082–10090 (2009).
5. A. V. Yulin and D. V. Skryabin, "Slowing down of solitons by intrapulse raman scattering in fibers with frequency cutoff," Opt. Lett. **31**, 3092–3094 (2006).
6. J. Lægsgaard, "Zero-velocity solitons in high-index photonic crystal fibers," J. Opt. Soc. Am. B **28**, 37–44 (2011).
7. J. P. Gordon, "Dispersive perturbations of solitons of the nonlinear Schrödinger-equation," J. Opt. Soc. Am. B **9**, 91–97 (1992).
8. S. M. J. Kelly, "Characteristic side-band instability of periodically amplified average soliton," Electron. Lett. **28**, 806–807 (1992).
9. Y. S. Kivshar, Z. Fei, and L. Vázquez, "Resonant soliton-impurity interactions," Phys. Rev. Lett. **67**, 1177–1180 (1991).
10. J. Leon, P. Anghel-Vasilescu, F. Ginovart, and N. Allegra, "Scattering of slow-light gap solitons with charges in a two-level medium," J. Phys. A: Math. Theor. **42**, 055101 (2009).
11. K. Stoychev, M. Primatarowa, and R. Kamburova, "Resonant scattering of nonlinear Schrodinger solitons from potential wells," Phys. Rev. E **70**, 066622 (2004).
12. S. Johnson, M. Povinelli, M. Soljacic, A. Karalis, S. Jacobs, and J. Joannopoulos, "Roughness losses and volume-current methods in photonic-crystal waveguides," Appl. Phys. B **81**, 283–293 (2005).
13. M. Patterson and S. Hughes, "Interplay between disorder-induced scattering and local field effects in photonic crystal waveguides," Phys. Rev. B **81** 245321 (2010).
14. S. Johnson, M. Ibanescu, M. Skorobogatiy, O. Weisberg, J. Joannopoulos, and Y. Fink, "Perturbation theory for Maxwell's equations with shifting material boundaries," Phys. Rev. E **65**, 066611 (2002).
15. G. P. Agrawal, *Nonlinear Fiber Optics* (Academic Press, San Diego, 2007).
16. J. Lægsgaard, "Theory of surface second-harmonic generation in silica nanowires," J. Opt. Soc. Am. B **27**, 1317–1324 (2010).
17. M. Sumetsky and Y. Dulashko, "Radius variation of optical fibers with angstrom accuracy," Opt. Lett. **35**, 4006–4008 (2010).